2017～2019年度 関西大学研究拠点形成支援経費研究成果報告書

著者	工藤 宏人, 宮前 翼, 上田 正人, 村山 憲弘, 林 順一, 松岡 光昭, 横山 佳帆, 大倉 滉平, 内藤 牧男, 下山 大輔, 関谷 亮, 灰野 岳晴, 池田 勝彦, 森 重雄, 土井 研児, 北垣 壽, 寺内 俊太郎, 五十井 浩平, 白杉 文香, 丸山 徹, Tamaki Mitsuyoshi, Nakamura Keisuke, Nakamura Gou, 齋藤 隆太, 仲村 利樹, 柳谷 仁志, Sakai Takahiro, 中本 光二, 山口 莉嘉, 藤田 智香, 福永 真理, 塩月 康平, 竹田 紘也, 山本 洋揮, 古澤 孝弘, 渡邊 健夫, 大隈 修, 前 一廣, 鈴木 一誓, 柿沼 綾子, 小俣 孝久, 坂本 貴則, 今坂 怜史, 石井 甫泰, 荒木 貞夫, 山本 秀樹, 大堀 静也, 小川 大貴, Kitagawa Kouta, 関 あずさ, Sonoc Alexandru, Jeswiet Jacob, 芝田 隼次
発行年	2020
権利	2-1 ネットワークポリマー事務局の許諾を得て公開しています。 2-4 日本金属学会の許諾を得て公開しています。 2-6 This is a post-peer-review, pre-copyedit version of an article published in International Journal of Metalcasting. The final authenticated version is available online at http://dx.doi.org/10.1007/s40962-019-00310-7. 2-7 This is a post-peer-review, pre-copyedit version of an article published in International Journal of Metalcasting. The final authenticated version is available online at: http://dx.doi.org/10.1007/s40962-018-00292-y. 2-13 This is the accepted version of the article, which has been published in final form at DOI 10.1016/j.micromeso.2018.07.005. 2-14 (C)フォトポリマー学会　この資料は著者最終...

Synthesis of CHA-type titanosilicate zeolites using titanium oxide as Ti source and evaluation of their physicochemical properties

Satoshi Imasaka, Hiroyasu Ishii, Jun'ichi Hayashi, Sadao Araki*, Hideki Yamamoto

Department of Chemical, Energy and Environmental Engineering, Faculty of Environmental and Urban Engineering, Kansai University, 3-3-35, Yamate-cho, Suita-shi, Osaka, 564-8680, Japan

ABSTRACT

To improve the physicochemical properties of CHA-type zeolites, we synthesized a CHA-type titanosilicate zeolite (Ti-CHA) with titanium instead of aluminum incorporated into its framework. Ti-CHA zeolites with various Si/Ti ratios were directly prepared by a 24-h hydrothermal reactions with the use of colloidal silica and titanium oxide as Si and Ti sources, respectively. A peak, assignable to isolated tetrahedrally coordinated Ti species, was clearly observed at ca. 220 nm in the UV–vis spectra of the Ti-CHA zeolite, confirming that titanium was incorporated into the zeolite framework. The effects of titanium content in the CHA zeolite on the thermal and acid stabilities were investigated. No changes were observed in the crystallinity, BET surface area, and micropore volume of a Ti-CHA zeolite with a Si/Ti ratio of 347, even after thermal treatment at 1150 °C. Furthermore, no changes were observed in the crystallinity of Ti-CHA zeolites with Si/Ti ratios of 45–347, after treatment with aqueous hydrochloric acid at 75 °C for 5 days. The amount of water adsorbed by the Ti-CHA zeolite with a Si/Ti ratio of 347 was lower than those of high-silica CHA-type zeolite with Si/Al=10 (Al-CHA zeolite) and pure-silica CHA-type zeolite (Si-CHA zeolite).

1. Introduction

Zeolites are widely used as separation materials, including adsorbents and separation membranes [1]. Recently, attention has been paid to CHA-type zeolites as separation materials with high separation performance and stability [2–4]. The CHA-type zeolite has an 8-membered ring window (0.38 nm×0.38 nm), which is the same as that of A-type zeolites. This window size is appropriate for separation of water/organic solvents and CO_2/CH_4 through molecular sieving effects [2–7]. Guest molecules can diffuse through the three-dimensional microporous structure of the CHA-type zeolite. Furthermore, CHA-type zeolites with a very wide range of Si/Al ratios from 2 to ∞ can be synthesized [3,4,8,9]. Therefore, it is possible to control the hydrophilic/hydrophobic nature of the material.

In recent years, applications of CHA type zeolites for CO_2 separation from natural gas, flue gas, and biogas have been studied [1]. However, these CO_2 separation processes are frequently humid conditions. Water is preferentially adsorbed by the polarity of the aluminum in the zeolite framework, leading to a decline of the CO_2 separation performance [6]. Thus, it is difficult to apply zeolites with a large amount of aluminum in their framework to CO_2 separation processes. High-silica CHA-type zeolites with high Si/Al ratios have been synthesized to enhance physicochemical properties such as acid and thermal stabilities, and hydrophobicity [10–12]. Takata et al. synthesized high-silica nanosized CHA-type zeolites with Si/Al=13–67 [12]. A Cu-loaded high-silica CHA-type zeolite catalyst exhibited good performance for NH3-SCR of NO_x even after hydrothermal treatment at 900 °C for 4 h. Furthermore, Miyamoto et al. synthesized a pure silica CHA type zeolite (Si/Al=∞) consisting entirely of silica and reported a high CO_2 adsorption capacity together with reduced effects of water [4,6]. Kida et al. synthesized a pure silica CHA-type zeolite membrane (Si/Al=∞), and the membrane showed a high CO_2 permeance of $>10^{-6}$ mol m^{-2} s^{-1} Pa^{-1} [13].

In addition, because CO_2 separation processes are performed under harsh conditions in high-pressure environments with coexisting hydrogen sulfide, further improvements to the physicochemical properties of zeolites are required [1]. Therefore, the substitution of aluminum into the zeolite framework with metals such as Ti, V, Ga, Fe, B, and Zn has attracted research attention [14–17]. TS-1 with titanium incorporated

into a MFI-type zeolite is already in practical use as a catalyst for liquid-phase oxidation reactions [14,18,19]. Recently, Kunitake et al. reported on the synthesis of Ti-CHA (Ti-Al-CHA) zeolites including Al and demonstrated thermal stability up to 1000 °C [20]. In that research, FAU-type zeolite as the starting material was subjected to the dealuminating treatment and Ti-FAU zeolite including Al was prepared by incorporating Ti via post synthesis. Thereafter, a Ti-Al-CHA zeolite was synthesized by interzeolite conversion. It was not possible to substitute all the Al in the CHA zeolite framework with Ti and this synthesis method required various complex processes. Eilersen et al. prepared a Ti-CHA zeolite completely free of Al in the framework by a direct hydrothermal treatment [21]. However, an expensive titanium (IV) ethoxide (TEOTi) precursor was used as the Ti source and a 4-day long hydrothermal treatment was necessary. In addition, the physical properties of the obtained Ti-CHA zeolite were not described in detail.

In this study, we synthesized CHA-type titanosilicate zeolites (Ti-CHA), without Al, from colloidal silica and titanium oxide as the Si and Ti sources, respectively. Using N, N, N-trimethtyl-1-adamantammonium hydroxide (TMAdaOH) as structure-directing agent (SDA), Ti-CHA zeolites with various Si/Ti ratios were prepared by the direct hydrothermal treatment for 24 h. The obtained Ti-CHA zeolites were thermally treated at 1150 °C and acid-treated by hydrochloric acid (HCl). After these treatments, the crystalline and pore structures of the Ti-CHA zeolites were compared with those of high-silica CHA-type zeolite (Al-CHA zeolite) with Si/Al=10 and pure silica CHA-type zeolite (Si-CHA zeolite). Finally, water adsorption measurements of Ti-CHA, Al-CHA, and Si-CHA zeolite were performed.

2. Experimental

2.1. Synthesis of Ti-CHA zeolite

Colloidal silica (40 wt%, Sigma-Aldrich) and titanium oxide (anatase-type, Wako Pure Chemical Industries Ltd.) were used as the Si and Ti sources, respectively. The mixture was prepared by mixing colloidal silica and titanium oxide. N,N,N-trimethyl-1-adamantane ammonium hydroxide (20 wt%, TMAdaOH, SACHEM, Inc.) was then added to the mixture. Thereafter, hydrofluoric acid (HF; 46% Wako Pure Chemical Industries Ltd.) was added until the solution pH became neutral. This solution was heated to evaporate water.

Finally, the synthetic gel was obtained at the desired gel composition by adding water (gel composition; 1 SiO_2: 0.018–0.067 TiO_2: 1.4 TMAdaOH: 1.4 HF: 6.0H_2O, Si/Ti ratio=15–57). The synthetic gel was transferred to a Teflon container, charged in an autoclave, and then hydrothermally treated at 150 °C for 24 h. The autoclave was removed from the oven and cooled to room temperature. The product was then recovered by filtration. The product was washed with distilled water, dried under reduced pressure for 24 h. Finally, the Ti-CHA zeolite was calcined in air at 700 °C (ramp rate of 1 °C min−1) to remove the SDA.

2.2. Synthesis of Al-CHA zeolite and Si-CHA zeolite

The high-silica CHA (Al-CHA) zeolite was prepared with a gel consisting of TMAdaOH (25 wt%, SACHEM, Inc.), Sodium hydroxide (Wako Pure Chemicals Industry Ltd.), and FAU-type zeolite (HSZ-360 HUA, HSZ-390 HUA, Tosoh Corp.) according to previous reports (gel composition; 1 SiO_2: 0.05 Al_2O_3: 0.2 TMAdaOH: 0.2 NaOH: 7.0H_2O) [22–24]. The synthetic gel was transferred to a Teflon container, charged into an autoclave, and then hydrothermally treated at 160 °C for 40 h. The autoclave was removed from the oven and cooled to room temperature and the product was recovered by centrifugation. The product was washed with distilled water, and this operation was repeated until the pH became neutral. The obtained product was dried at room temperature. The Al-CHA zeolite was calcined in air at 700 °C (ramp rate of 1 °C min−1) to remove the SDA.

The Si-CHA zeolite was synthesized in the same way as the Ti-CHA zeolite with a gel consisting of TMAdaOH (20 wt%, SACHEM, Inc.), hydrofluoric acid (HF; Wako Pure Chemical Industries Ltd.), and colloidal silica (40 wt%, Sigma-Aldrich). The gel composition was 1 SiO_2: 1.4 TMAdaOH: 1.4 HF: 6.0H_2O.

2.3. Characterization

The crystal structures of the Ti-CHA zeolites were confirmed by Xray diffraction (XRD, Rigaku, RINT TTR3) using Cu Ka radiation, and operated at 40 kV and 30 mA. The morphology and size were observed with a field emission scanning electron microscope (FE-SEM, Hitachi high technology, S-4800). The chemical species of

Ti in the framework of the CHA zeolite were analyzed by Fourier-transform infrared (FT-IR, Shimadzu, IR Affinity-1S), and ultraviolet–visible light (UV–vis, JASCO corp., V-550). FT-IR spectra were obtained by the KBr method. UV–vis spectra were obtained from diffuse reflection reflectance referenced against MgO as the baseline. The diffuse reflection spectra were converted into absorption spectra by the Kubelka–Munk function. The Si/Ti ratios of Ti-CHA zeolites were determined with the use of inductively coupled plasma optical emission spectroscopy (ICP, Shimadzu, ICPS-7510). For the BET specific surface area and micropore volume, nitrogen adsorption isotherms were measured at liquid nitrogen temperature (Microtrac BEL, BELSORP). The sample pre-treatment was carried out at 200 °C for 1 h. The specific surface areas were calculated by the Brunauer–Emmett–Teller method (BET) from nitrogen isotherms. The BET specific surface area in this study was treated as BET equivalent surface areas based on IUPAC. Furthermore, the micropore volumes (Vmicro) were also calculated by the t-plot method from the nitrogen isotherms [8,13].

2.4. Thermal and acid stability testing and water adsorption measurements

The physicochemical stabilities of the CHA-type zeolites were evaluated. About 2 g of the CHA-type zeolites were thermally treated in air at 1000–1150 °C for 24 h (ramp rate of 1 °C min−1). Furthermore, the acid stabilities of CHA-type zeolites were investigated by treatment with 5M aqueous hydrochloric acid (HCl) at 75 °C for 5 days. 0.2 g of zeolite was immersed in 40 ml of 5M HCl solution at 75 °C for 5 days. After these treatments, the crystallinity, pore structure, and chemical form of Ti species and the Si/Ti ratio of Ti-CHA zeolites were analyzed from XRD patterns, nitrogen isotherms, UV–vis spectra, and ICP, respectively.

The water adsorption measurements of the CHA-type zeolites were carried out at 40 °C (Microtrac BEL, Belsorp-max). The sample pretreatment was carried out at 120 °C for 24 h. The water adsorption amount was determined from water isotherms.

3. Results and discussion

3.1. Characteristics of Ti-CHA zeolite

The XRD patterns of the products prepared at a Si/Ti ratio of 15–57 and the various TiO_2 are shown in Fig. 1.

The CHA-type zeolite structure was determined to be a homogeneous phase for all the products, and the formation of CHA zeolite was confirmed. We found that a higher gel Si/Ti ratio produced a higher crystallinity in the obtained CHA zeolite. Furthermore, no peaks related to TiO_2 were observed, suggesting that Ti species were present in the framework of the CHA zeolite. The chemical composition, BET specific surface area, and micropore volume of the CHA zeolite prepared in this study are listed in Table 1. By increasing the Si/Ti ratio of the gel to 15–57, the Si/Ti ratio of the Ti-CHA zeolite increased to be in the range of 45–578 (Samples 1–3). Subsequently, the BET specific surface area and the micropore volume showed almost no differences regardless of the Si/Ti ratio.

The FE-SEM images of the obtained Ti-CHA zeolites (Samples 1–3) are shown in Fig. 2. The morphology of these samples was cubic, as is typical for CHA zeolites and their particle sizes were in the range of 2–8 μm.

The chemical species of Ti in the framework of the CHA-type zeolites were analyzed by FT-IR and UV–vis. Fig. 3 shows the FT-IR spectra of the Ti-CHA zeolites. A very weak band at ca. 970 cm−1 was observed for all the Ti-CHA zeolites, relating to Si-O-Ti bond [25–28]. This result suggests that Ti was incorporated into the zeolite framework. Fig. 4 shows the UV–vis spectra of the Ti-CHA zeolite. The peak at ca. 220 nm was assigned to isolated tetrahedrally coordinated Ti species, and was found for all the Ti-CHA zeolites, confirming the incorporation of Ti into the zeolite framework [14,20]. However, a peak was also observed at ca. 330 nm for all the Ti-CHA zeolites, suggesting the presence of anatase TiO_2, as shown in Fig. 4 (d) [14]. Thus, some Ti species were not incorporated into the zeolite framework. It is possible that the TiO_2 used as the Ti source persisted as small particles and clusters that could not be detected by the XRD.

The Ti species of the Ti-CHA zeolites were confirmed by the peaks at ca. 220 and ca. 330 nm in the UV–vis spectra. The peak ratio was calculated as the peak height at ca. 320 nm divided by the peak height at ca. 220 nm. The peak ratios of Samples 1–3 were 0.39, 0.07, and 0.05, respectively. Sample 1 (Si/Ti=45) contained a large amount of anatase TiO_2 and Ti species of Sample 3 (Si/Ti=578) were mainly incorporated into the CHA-type zeolite framework.

3.2. Evaluation of thermal stability

The thermal stabilities of the CHA-type zeolites (Samples 1–5) were evaluated. The XRD patterns before and after the thermal treatment are shown in Fig. 5. The crystal structure of the Al-CHA zeolite (Sample 4) collapsed following the thermal treatment at 1000 °C. The crystal structure of the zeolites likely collapsed because of the desorption of Al from the framework.

The crystal structures of the Ti-CHA zeolites (Samples 1–3) and the Si-CHA zeolite (sample 5) were maintained even after the thermal treatment at 1150 °C, and an improvement of the thermal stability was expected owing to the Al free in the zeolite framework. In Sample 2 (Si/Ti=347), no change of the peak intensity was found.

Table 2 lists the BET specific surface area and the micropore volume of the CHA-type zeolites (Sample 1–5) before and after the thermal treatment. At 1150 °C, the BET specific surface area and the micropore volume of the Si-CHA zeolite (Sample 5) decreased. In contrast, no changes were observed in either the BET specific surface area or the micropore volume of the Ti-CHA zeolite (Sample 2). Thus, we confirmed that the thermal stability of the CHA-type zeolite was improved by the incorporation of Ti into the framework. Kunitake et al. synthesized a Ti-Al-CHA zeolite having a thermal stability as high as 1000 °C [20]. The Ti-CHA zeolite synthesized in this study showed higher thermal stability than that of Ti-Al-CHA zeolite. However, the BET specific surface area and micropore volume decreased in Sample 1 (Si/Ti=45) and Sample 3 (Si/Ti=578) after the thermal stability testing at 1150 °C.

Fig. 6 shows the UV–vis spectra of rutile TiO2 and Ti-CHA zeolite (Samples 1–3) after the thermal treatment. Another peak was observed at ca. 380 nm in Sample 1 (Si/Ti=45) after the thermal treatment, in addition to the peaks at ca. 220 nm and ca. 330 nm relating to the isolated tetrahedrally coordinated Ti species and anatase TiO_2, respectively. This result suggested the presence of rutile TiO_2. The decrease of the BET specific surface area and micropore volume in Sample 1 after the thermal treatment at 1150 °C was likely caused by the transformation of the anatase TiO_2 into rutile TiO_2. When anatase TiO_2 is heated to 900 °C or above, it is known to transform to rutile TiO_2. In addition, it is also considered that the isolated tetrahedrally coordinated Ti species in the zeolite framework was removed. Then, the aggregation and transformation to the

anatase TiO_2 may be occurred. Therefore, the zeolite pore structure of Sample 1 changed after the thermal treatment at 1150 °C. In Sample 2 (Si/Ti=347) and Sample 3 (Si/Ti=578), no peaks from rutile TiO_2 were observed. However, because only a small amount of the anatase TiO_2 was present in samples 2 and 3, the rutile TiO_2 might not be detectable in the UV–vis spectra. It is considered that the decrease in the BET specific surface area and micropore volume of Sample 3 due to the thermal treatment at 1150 °C can be simply attributed to the small amount of Ti in the zeolite framework. Thus, we found that the Ti-CHA zeolite was stable up to 1150 °C in the synthesis method of this study compared previously reported Al-CHA zeolite and Si-CHA zeolite. The optimum Si/Ti ratio in this preparation condition was 347 regarding the thermal stability.

3.3. Evaluation of acid stability

Fig. 7 shows the XRD patterns of CHA-type zeolite (Sample 1–5) before and after the acid treatment. The crystallinity of the Al-CHA zeolite (Sample 4) decreased after treatment with the 5M HCl solution, owing to the acid leaching Al from the zeolite, which decomposed its framework structure [29]. The crystal structure of the Ti-CHA zeolite (Samples 1–3) and the Si-CHA zeolite (sample 5) were maintained after the HCl treatment at 75 °C for 5 days. We found that the CHA-type zeolite without Al had excellent stability to acid.

Table 3 lists the BET specific surface areas and micropore volumes of the CHA-type zeolites (Samples 1–5) before and after the acid treatment. We observed that the BET specific surface areas and the micropore volume increased in Sample 2 (Si/Ti=347) and Sample 3 (Si/Ti=578).

Fig. 8 shows the Si/Ti ratio of Ti-CHA zeolites (samples 1–3) before and after acid treatment. The Si/Ti ratio in Sample 1 increased from 45 to 68 after acid treatment in ICP analysis. Conversely, the Si/Ti ratios of Sample 2 and Sample 3 decreased from 347 to 578 to 304 and 478, respectively. Hence, it is considered that the amount of Ti decreased in Sample 1 and the amount of Si decreased in Samples 2 and 3 by acid treatment.

Fig. 9 shows the UV–vis spectra of the Ti-CHA zeolites (Samples 1–3) after the acid treatment. Peaks, assignable to isolated tetrahedrally coordinated Ti species, were clearly observed at ca. 220 nm in the UV–vis spectra of all Ti-CHA zeolites after the acid treatment [14,20]. Thus, we confirmed that Ti was present in the CHA-type zeolite framework. The Ti species of the Ti-CHA zeolites were similarly discussed in terms of the

peak ratio at ca. 220 nm and ca. 330 nm relating to isolated tetrahedrally coordinated Ti species and the anatase TiO_2, respectively. The peak ratios of Samples 1–3 were 0.19, 0.05, and 0.02, respectively, although the peak ratios before the acid treatment were 0.38, 0.07, and 0.05, respectively. The peak ratios of all the Ti-CHA zeolites were lower than those before the acid treatment. These changes indicate that the amount of anatase TiO_2 in the zeolite was reduced by the acid treatment.

The results of the Si/Ti ratio and UV–vis spectra after acid treatment suggest that small amounts of anatase TiO_2 and Si species were present in the Ti-CHA zeolite pores and on the outer surface zeolite. We suspected that the increases of the BET specific surface area and the micropore volume in Samples 2 and 3 after the acid treatment were caused by a reduction in the amounts of anatase TiO_2 and Si species in the zeolite pores and on the outer surface zeolite. We found that the BET surface area and pore volume of the Ti-CHA zeolite could be increased by the acid treatment.

3.4. Comparison of amount of water adsorbed

Fig. 10 shows water adsorption isotherms measured at 40 °C for the Ti-CHA zeolite (Sample 2), the Al-CHA zeolite (Sample 4), and the Si- CHA zeolite (Sample 5). The amount of adsorbed water for the Al-CHA zeolite was the highest among the three zeolites. It is known that the silicon, aluminum, oxygen atoms in zeolite framework as well as cation located in zeolite pore have the partial charges [30]. Thus, H_2O was likely adsorbed onto the Al-CHA zeolite by strong interactions. The amount of water adsorbed to the Si-CHA zeolite was considerable less than that adsorbed to the Al-CHA zeolite. This result was attributed to the hydrophobic pore system because the framework consists of Si-O-Si bonds [13]. Furthermore, although the BET specific surface area and micropore volume of the Ti-CHA zeolite were larger than those of the Si-CHA zeolite, the amount of water adsorption was reduced. These results suggest that the pore system based on Si-O-Ti bonds had a higher hydrophobicity than that based on Si-O-Si bonds. The pores of the Si-CHA zeolite may be slightly more hydrophilic than the pores of the Ti-CHA zeolite. In addition, although the peak intensities in the XRD patterns were almost the same, the crystallinity of the Si-CHA zeolite might be lower than that of the Ti-CHA zeolite. Thus, silanol groups might have been generated in the Si-CHA zeolite compared with the Ti-CHA zeolite [4,13].

4. Conclusion

In this study, CHA-type titanosilicate zeolites (Ti-CHA) with various Si/Ti ratios were synthesized by a 24-h reaction with the use of inexpensive colloidal silica and titanium oxide as Si and Ti sources, respectively. The Ti-CHA zeolite showed excellent thermal and acid stability at 1150 °C and 5M HCl, respectively. It was demonstrated that the thermal stability and hydrophobicity of Ti-CHA zeolite was higher than those of reported Al-CHA zeolite and Si-CHA zeolite. The optimum Si/Ti ratio of the Ti-CHA zeolite in this synthesis condition was 347 regarding the thermal stability. Furthermore, the water adsorption amount with the Si/Ti of 347 was the lowest among the high-silica CHA-type zeolites (Al-CHA) and pure-silica CHA-type zeolites (Si-CHA) synthesized in this study. These results indicate that the Ti-CHA zeolite is a promising material for gas separation processes that operate in the presence of water and hydrogen sulfide.

Appendix A. Supplementary data

Supplementary data related to this article can be found at https://doi.org/10.1016/j.micromeso.2018.07.005.

References

[1] N. Kosinov, J. Gascon, F. Kapteijn, E.J.M. Hensen, J. Membr. Sci. 499 (2016) 65–79.

[2] Y. Hasegawa, C. Abe, F. Mizukami, Y. Kowata, T. Hanaoka, J. Membr. Sci. 415 (2012) 368–374.

[3] J. Shang, G. Li, R. Singh, P. Xiao, J.Z. Liu, P.A. Webley, J. Phys. Chem. C 117 (2013) 12841–12847.

[4] M. Miyamoto, T. Nakatani, Y. Fujioka, K. Yogo, Microporous Mesoporous Mater. 206 (2015) 67–74.

[5] N. Kossinov, C. Auffret, G.J. Borghuis, V.G.P. Sripathi, E.J.M. Hensen, J. Membr. Sci. 484 (2015) 140–145.

[6] M. Miyamoto, Y. Fujiokax, K. Yogo, J. Mater. Chem. 22 (2012) 20186–20189.

[7] N. Kosinov, C. Auffret, C. Gucuyener, B.M. Szyja, J. Gascon, F. Kapteijn, E.J.M. Hensen, J. Mater. Chem. A 2 (2014) 13083–13092.

[8] Q. Zhu, J.N. Kondo, R. Ohnuma, Y. Kubota, M. Yamaguchi, T. Tatsumi, Microporous Mesoporous Mater. 112 (2008) 153–161.

[9] B. Liu, Y. Zheng, N. Hu, T. Gui, Y. Li, F. Zhang, R. Zhou, X. Chen, H. Kita, Microporous Mesoporous Mater. 196 (2014) 270–276.

[10] M. Itakura, T. Inoue, A. Takahashi, T. Fujitani, Y. Oumi, T. Sano, Chem. Lett. 37 (2008) 908–909.

[11] M. Itakura, I. Goto, A. Takahashi, T. Fujitani, Y. Ide, M. Sadakane, T. Sano, Microporous Mesoporous Mater. 144 (2011) 91–96.

[12] T. Takata, N. Tsunoji, Y. Takamitsu, M. Sadakane, T. Sano, Microporous Mesoporous Mater. 225 (2016) 524–533.

[13] K. Kida, Y. Maeta, K. Yogo, J. Membr. Sci. 522 (2017) 363–370.

[14] M. Tamura, W. Chaikittisilp, T. Yokoi, T. Okubo, Microporous Mesoporous Mater. 112 (2008) 202–210.

[15] Q.-H. Xia, T. Tatsumi, Mater. Chem. Phys. 89 (2005) 89–98.

[16] V.R. Choudhary, S.K. Jana, Appl. Catal. Gen. 224 (2002) 51–62.

[17] P. Wu, T. Komatsu, T. Yashima, J. Phys. Chem. 100 (1996) 10316–10322.

[18] Y. Han, H.S. Zehng, N. Guan, Catal. Commun. 3 (2002) 221–225.

[19] X. Meng, W. Fan, Y. Kubota, T. Tatsumi, J. Catal. 244 (2006) 192–198.

[20] Y. Kunitake, T. Takata, Y. Yamasaki, N. Yamanaka, N. Tsunoji, Y. Takamitsu, M. Sadakane, T. Sano, Microporous Mesoporous Mater. 215 (2015) 58–66.

[21]E.A. Eilertsen, S. Bordiga, C. Lamberti, A. Damin, F. Bonino, B. Arstad, S. Svelle, U. Olsbye, K.P. Lillerud, ChemCatChem 3 (2011) 1869–1871.

[22] Y. Hasegawa, C. Abe, T. Ikeda, K. Sato, S. Imasaka, M. Itakura, K. Yano, Adv. Porous Mater 4 (2016) 134–143.

[23] N. Yamanaka, M. Itakura, Y. Kiyozumi, Y. Ide, M. Sadakane, T. Sano, Microporous Mesoporous Mater. 158 (2012) 141–147.

[24] N. Yamanaka, M. Itakura, Y. Kiyozumi, M. Sadakane, T. Sano, Bull. Chem. Soc. Jpn. 86 (2013) 1333–1340.

[25] C.-H. Huang, H. Bai, S.-L. Liu, Y.-L. Huang, Micro & Nano Lett. 6 (2011) 646–649.

[26] X. Gao, I.E. Wachs, Catal. Today 51 (1999) 233–254.

[27] C. He, B. Tian, J. Zhang, J. Colloid Interface Sci. 344 (2010) 382–389.

[28] M. Zhang, L. Shi, S. Yuan, Y. Zhan, J. Fang, J. Colloid Interface Sci. 330 (2009) 113–118.

[29] Y. Cui, H. Kita, K. Okamoto, J. Membr. Sci. 236 (2004) 17–27.

[30] P. Bai, P. Ghosh, J.C. Sung, D. Kohen, J.I. Siepmann, R.Q. Snurr, Fluid Phase Equil. 336 (2014) 146–151.

Captions

Fig. 1. XRD patterns of (a) Ti-CHA zeolite (Si/Ti=15), (b) Ti-CHA zeolite (Si/Ti=30), (c) Ti-CHA zeolite (Si/Ti=57), (d) Anatase TiO_2, (e) Rutile TiO_2, (f)Brookite TiO_2.

Fig. 2. FE-SEM images of (a) Ti-CHA zeolite (Sample 1), (b) Ti-CHA zeolite (Sample 2), and (c) Ti-CHA zeolite (Sample 3).

Fig. 3. FT-IR spectra of (a) Ti-CHA zeolite (Sample 1), (b) Ti-CHA zeolite (Sample 2), (c) Ti-CHA zeolite (Sample 3), and (d) Si-CHA zeolite (Sample 5).

Fig. 4. UV–vis spectra of (a) Ti-CHA zeolite (Sample 1), (b) Ti-CHA zeolite (Sample 2), (c) Ti-CHA zeolite (Sample 3). and (d) Anatase TiO_2.

Fig. 5. XRD patterns of various CHA zeolites after thermal treatment at 1000–1150 °C. (a) Al-CHA zeolite (Sample 4), (b) Si-CHA zeolite (Sample 5), (c) Ti-CHA zeolite (Sample 1), (d) Ti-CHA zeolite (Sample 2), and (e) Ti-CHA zeolite (Sample 3).

Fig. 6. UV–vis spectra of (a) Ti-CHA zeolite (Sample 1), (b) Ti-CHA zeolite (Sample 2), (c) Ti-CHA zeolite (Sample 3) after thermal treatment at 1150 °C, (d) Rutile TiO_2.

Fig. 7. XRD patterns of various CHA zeolites after acid treatment with HCl solution at 75 °C for 5 days. (a) Al-CHA zeolite (Sample 4), (b) Si-CHA zeolite (Sample 5), (c) Ti-CHA zeolite (Sample 1), (d) Ti-CHA zeolite (Sample 2), and (e) Ti-CHA zeolite (Sample 3).

Fig. 8. Si/Ti ratio of Ti-CHA zeolite (Samples 1–3) before and after acid treatment with HCl solution at 75 °C for 5 days.

Fig. 9. UV–vis spectra of (a) Ti-CHA zeolite (Sample 1), (b) Ti-CHA zeolite (Sample 2), (c) Ti-CHA zeolite (Sample 3) after acid treatment with HCl solution at 75 °C for 5 days.

Fig. 10. H_2O adsorption isotherms of (a) Al-CHA zeolite (Sample 4), (b) Si-CHAzeolite (Sample 5), and (c) Ti-CHA zeolite (Sample 2) at 40 °C.

Table 1 Physicochemical properties of various CHA zeolites.

Table 2 BET Surface area and micropore volume of CHA zeolites after thermal treatment at 1150 °C.

Table 3 BET Surface area and micropore volume of CHA zeolites after acid treatment with HCl solution at 75 °C for 5 days.

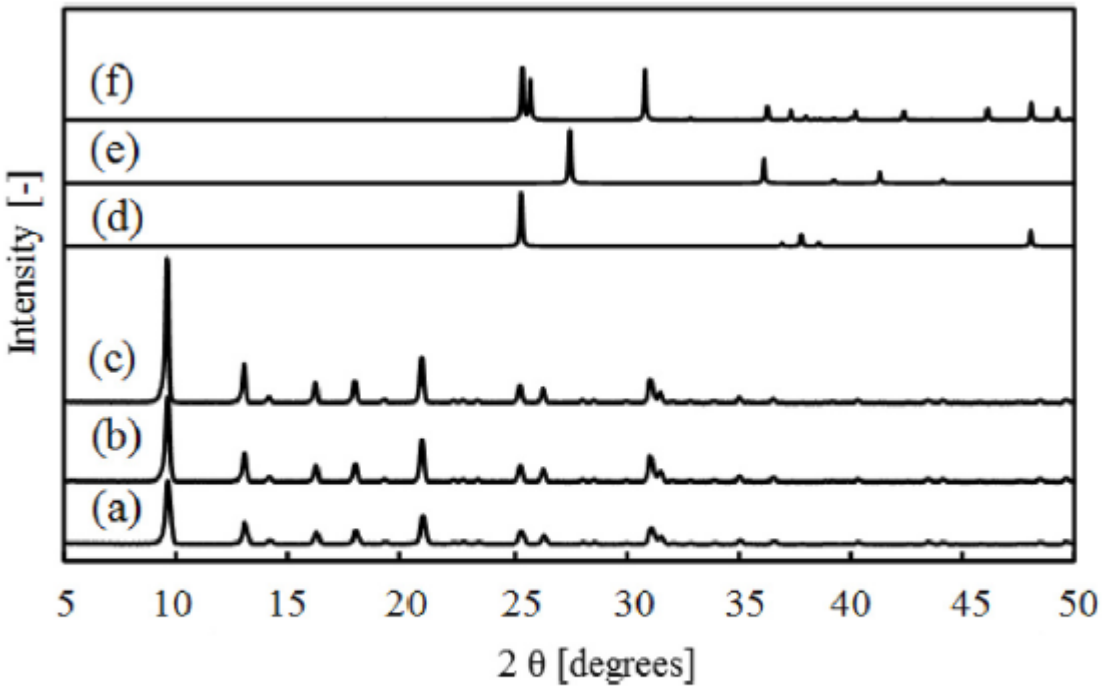

Fig. 1. XRD patterns of (a) Ti-CHA zeolite (Si/Ti = 15), (b) Ti-CHA zeolite (Si/Ti = 30), (c) Ti-CHA zeolite (Si/Ti = 57), (d) Anatase TiO_2, (e) Rutile TiO_2, (f) Brookite TiO_2.

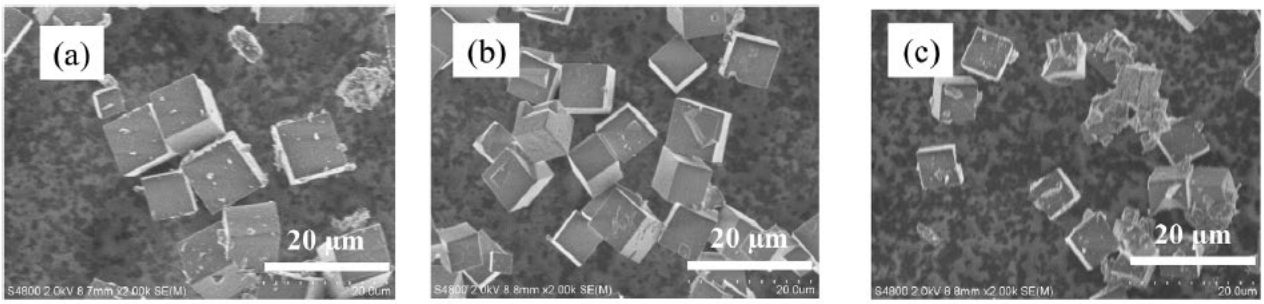

Fig. 2. FE-SEM images of (a) Ti-CHA zeolite (Sample 1), (b) Ti-CHA zeolite (Sample 2), and (c) Ti-CHA zeolite (Sample 3).

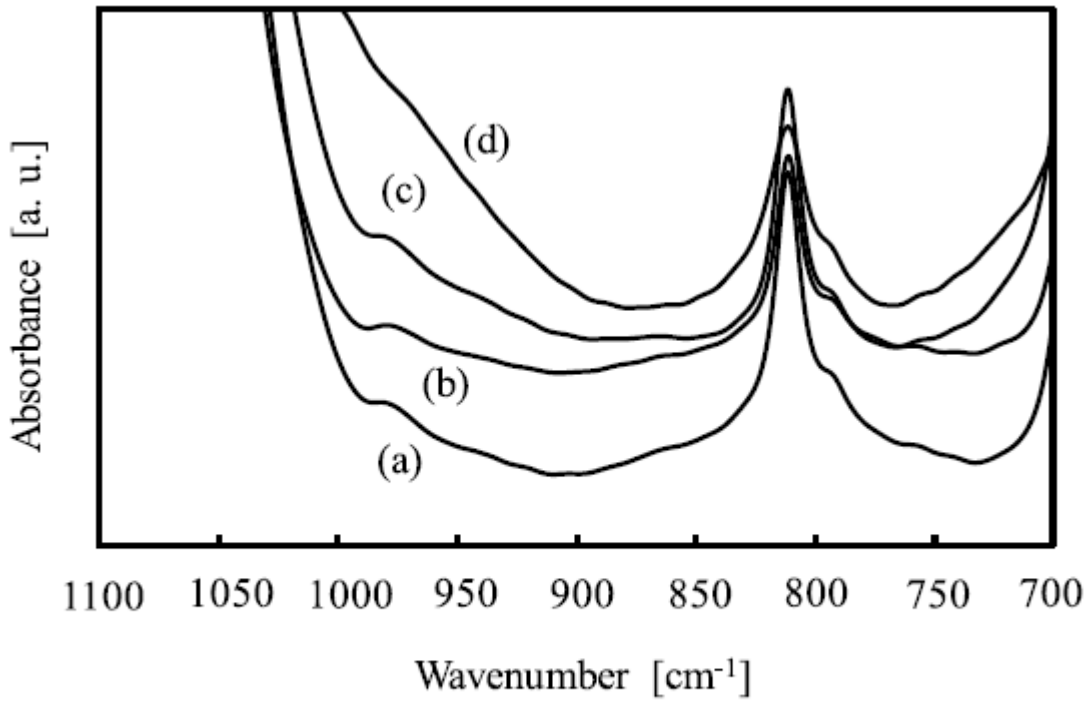

Fig. 3. FT-IR spectra of (a) Ti-CHA zeolite (Sample 1), (b) Ti-CHA zeolite (Sample 2), (c) Ti-CHA zeolite (Sample 3), and (d) Si-CHA zeolite (Sample 5).

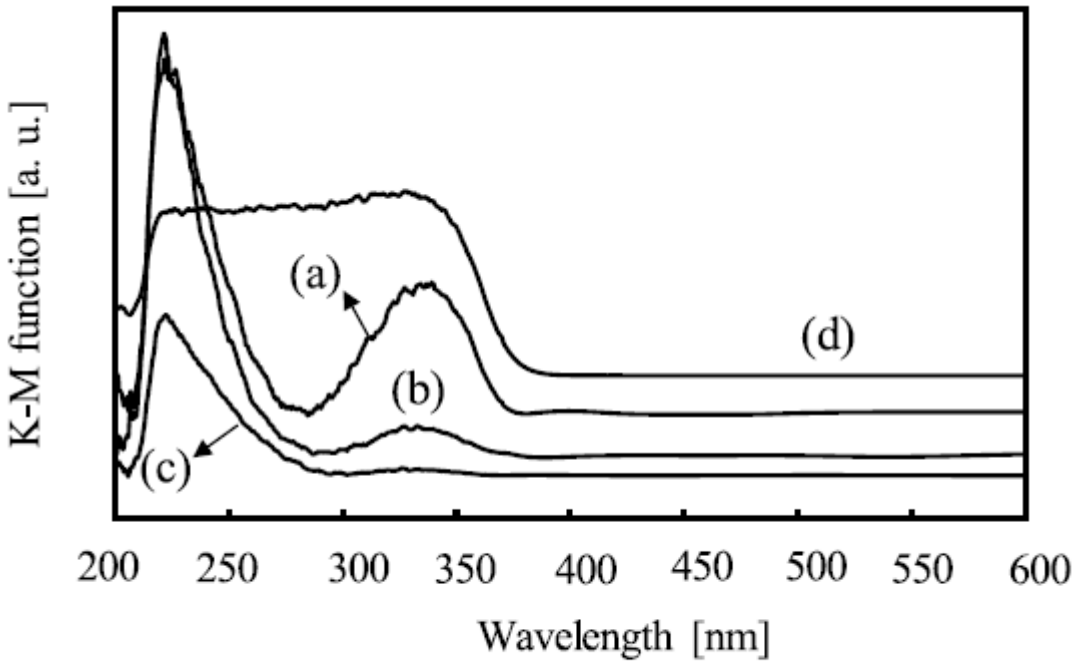

Fig. 4. UV–vis spectra of (a) Ti-CHA zeolite (Sample 1), (b) Ti-CHA zeolite (Sample 2), (c) Ti-CHA zeolite (Sample 3). and (d) Anatase TiO_2.

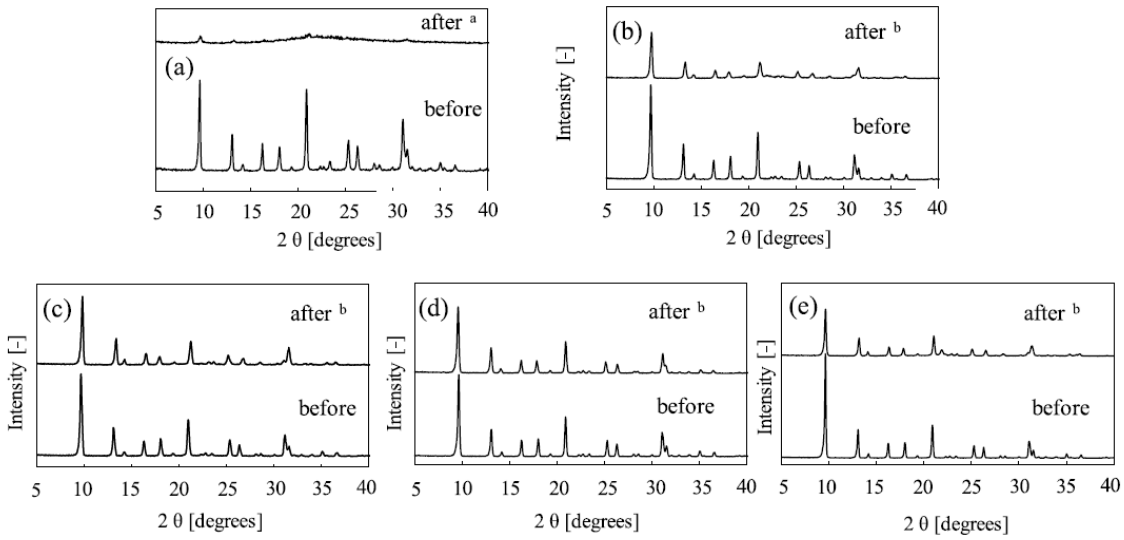

Fig. 5. XRD patterns of various CHA zeolites after thermal treatment at 1000–1150 °C. (a) Al-CHA zeolite (Sample 4), (b) Si-CHA zeolite (Sample 5), (c) Ti-CHA zeolite (Sample 1), (d) Ti-CHA zeolite (Sample 2), and (e) Ti-CHA zeolite (Sample 3).

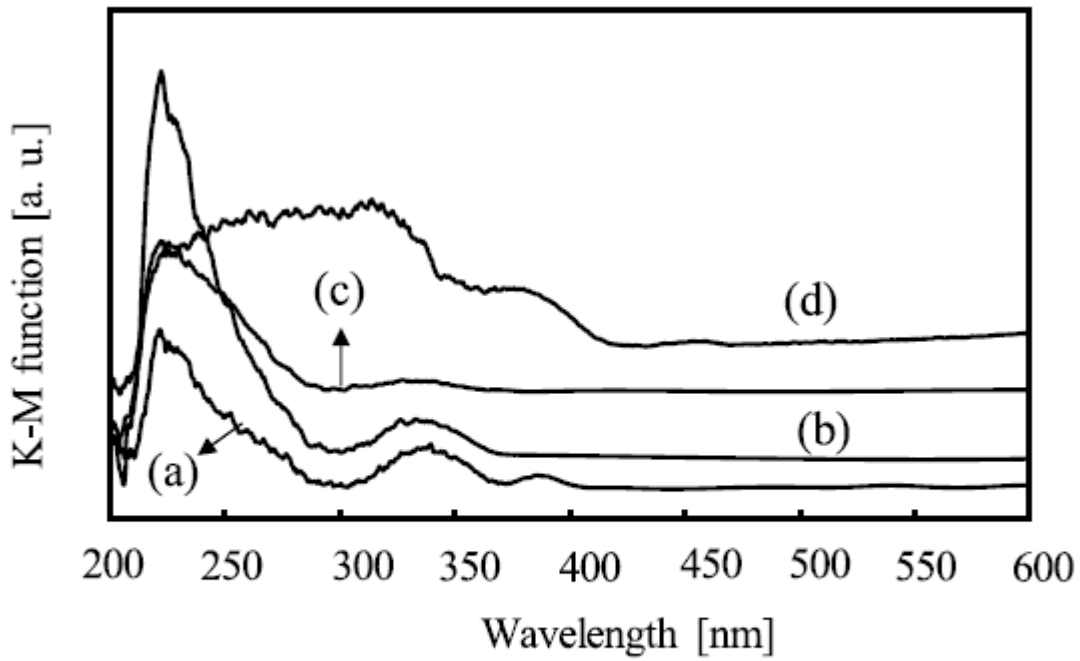

Fig. 6. UV–vis spectra of (a) Ti-CHA zeolite (Sample 1), (b) Ti-CHA zeolite (Sample 2), (c) Ti-CHA zeolite (Sample 3) after thermal treatment at 1150 °C, (d) Rutile TiO_2.

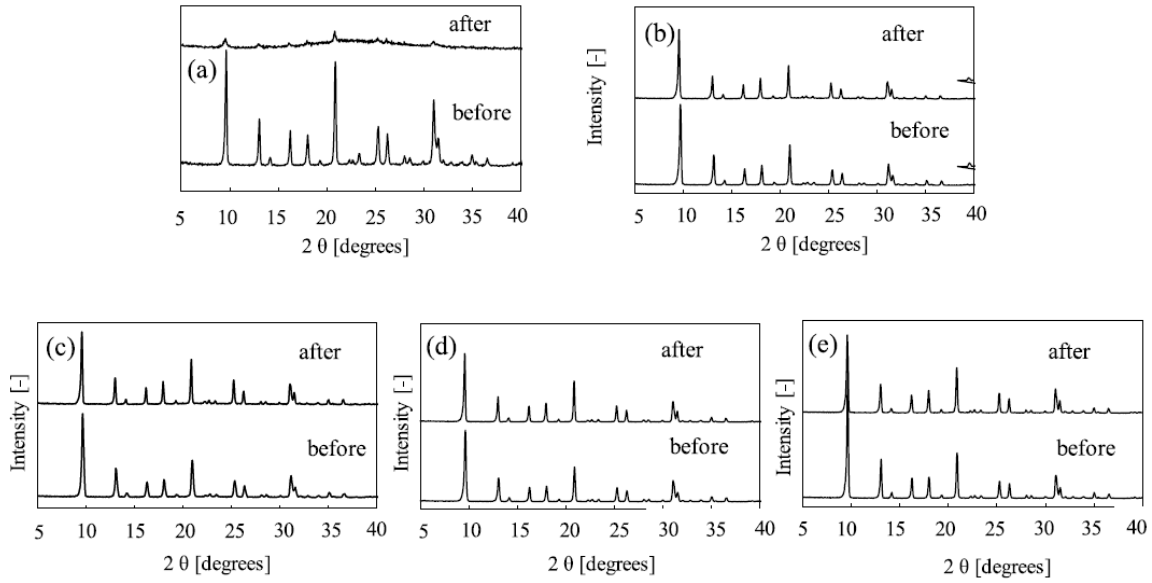

Fig. 7. XRD patterns of various CHA zeolites after acid treatment with HCl solution at 75 °C for 5 days. (a) Al-CHA zeolite (Sample 4), (b) Si-CHA zeolite (Sample 5), (c) Ti-CHA zeolite (Sample 1), (d) Ti-CHA zeolite (Sample 2), and (e) Ti-CHA zeolite (Sample 3).

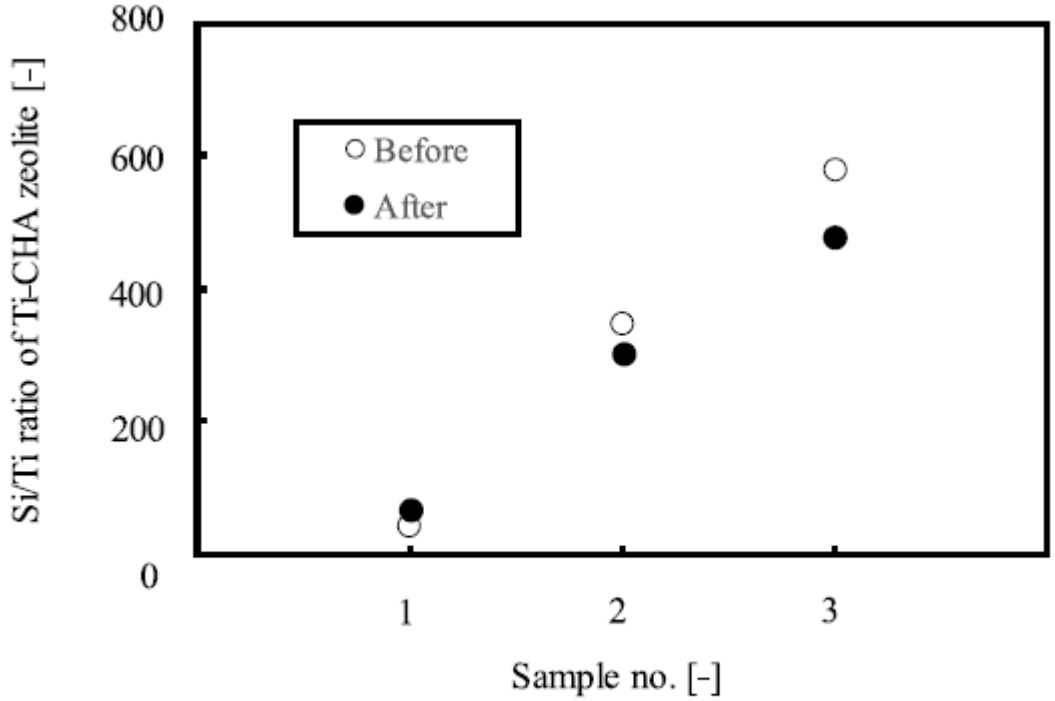

Fig. 8. Si/Ti ratio of Ti-CHA zeolite (Samples 1–3) before and after acid treatment with HCl solution at 75 °C for 5 days.

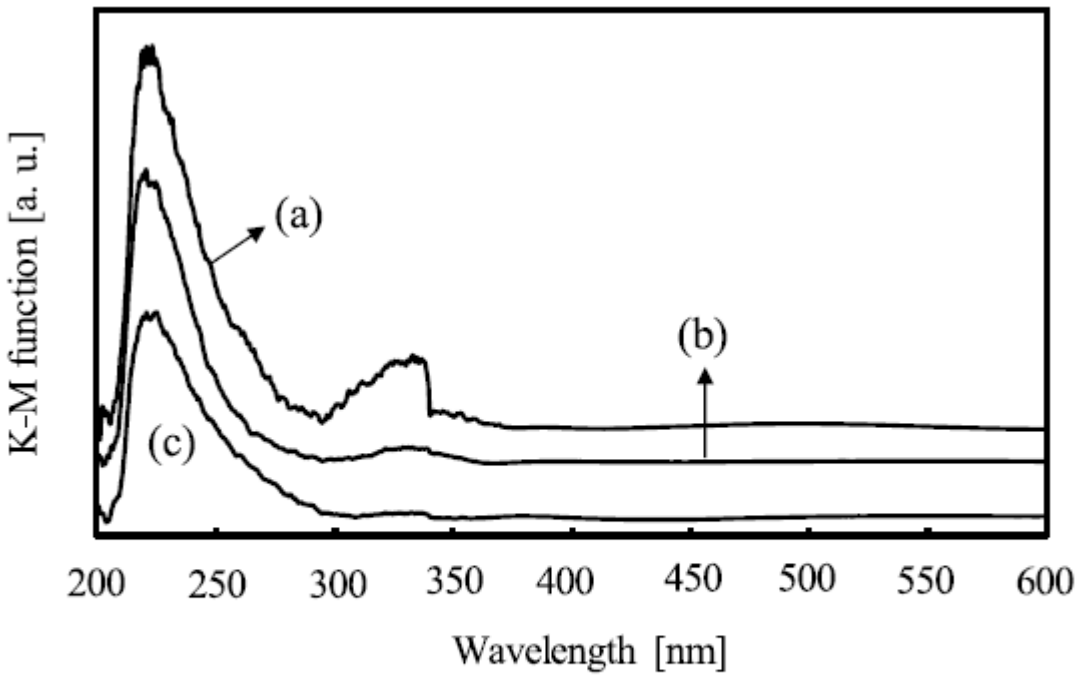

Fig. 9. UV–vis spectra of (a) Ti-CHA zeolite (Sample 1), (b) Ti-CHA zeolite (Sample 2), (c) Ti-CHA zeolite (Sample 3) after acid treatment with HCl solution at 75 °C for 5 days.

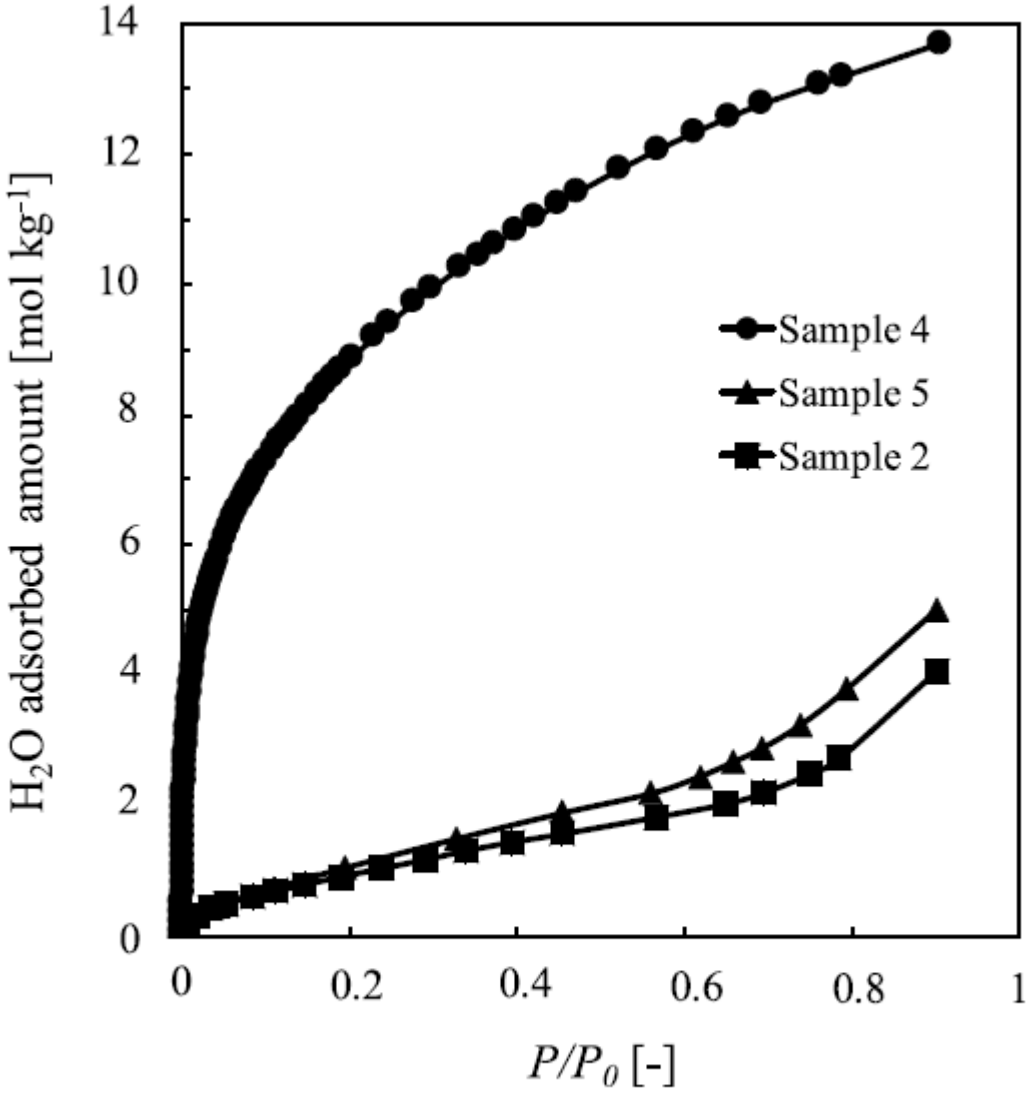

Fig. 10. H_2O adsorption isotherms of (a) Al-CHA zeolite (Sample 4), (b) Si-CHA zeolite (Sample 5), and (c) Ti-CHA zeolite (Sample 2) at 40 °C.

Table 1
Physicochemical properties of various CHA zeolites.

Sample	Synthesis gel		Product			
	Si/Ti	Si/Al	Si/Ti	Si/Al	S_{BET} [$m^2\ g^{-1}$]	V_{micro} [$cm^3\ g^{-1}$]
1	15	–	45	–	863	0.302
2	30	–	347	–	813	0.295
3	57	–	578	–	883	0.314
4	–	10	–	11	776	0.277
5	∞	∞	∞	∞	714	0.250

Table 2
BET Surface area and micropore volume of CHA zeolites after thermal treatment at 1150 °C.

	Sample 1		Sample 2		Sample 3		Sample 4		Sample 5	
	before	after	before	after	before	after	before	after	before	after
S_{BET} [$m^2\ g^{-1}$]	863	557	813	819	883	689	776	238	714	462
V_{micro} [$cm^3\ g^{-1}$]	0.302	0.194	0.295	0.286	0.314	0.242	0.277	4.58×10^{-3}	0.250	0.160

Table 3
BET Surface area and micropore volume of CHA zeolites after acid treatment with HCl solution at 75 °C for 5 days.

	Sample 1		Sample 2		Sample 3		Sample 4		Sample 5	
	before	after	before	after	before	after	before	after	before	after
S_{BET} [$m^2\ g^{-1}$]	863	763	813	980	883	985	776	77.2	714	696
V_{micro} [$cm^3\ g^{-1}$]	0.302	0.273	0.295	0.354	0.314	0.351	0.277	0.037	0.250	0.242